

High-performance MPPT control of DFIG with optimized flux reference in presence of nonlinear magnetic characteristic

Youssef Majdoub, Ahmed Abbou, Mohamed Akherraz

Mohammed V University in Rabat, Rabat, Morocco
Mohammadia School of Engineers, Agdal Rabat, Morocco

Article Info

Article history:

Received Oct 29, 2021

Revised April 20, 2022

Accepted May 2, 2022

Keywords:

Backstepping control

DFIG

High-performance MPPT

Iron losses

Magnetic saturation

Optimization

ABSTRACT

In recent years, an expansive research exertion has been devoted to the control for aerogenerators conforming of a Doubly Fed Induction Generator (DFIG) coupled to a wind turbine. Most preceding controllers based on standard models (whose magnetic induction characteristic is considered linear and iron losses have not been taken into account). Since such a magnetic characteristic is nonlinear in practice, this work develops a variable speed control strategy on the basis of a DFIG model in presence of nonlinear magnetic characteristic and iron losses. The main contribution of this paper is to present a high-performance maximum power point (MPPT) control of DFIG based on rotor flux optimization, designed to reach an optimal operational condition. Of the foregoing, the control goal is twofold: i) minimization of the stator and rotor currents circulating by controlling the rotor flux for a maximum electromagnetic torque; and ii) captured the maximum wind power to insure the attainment of MPPT. The performances of the proposed command has been studied theoretically and validated by simulation studies with MATLAB/Simulink.

This is an open access article under the [CC BY-SA](https://creativecommons.org/licenses/by-sa/4.0/) license.



Corresponding Author:

Youssef Majdoub

Mohammed V University in Rabat, Mohammadia School of Engineers

Agdal Rabat, Morocco

Email: youssefmajdoub@research.emi.ac.ma

1. INTRODUCTION

Global warming and lowering fossil reserves have pushed many countries to move towards the use of renewable energies, which are considered clean energy [1]-[4]. In this context, the major areas of research in the world have been focused on the problem of optimizing wind energy captured by the turbine. Admittedly, the control of a wind turbine equipped with a fixed-speed alternator is very simple but can no longer ensure optimization of the aerodynamic energy captured. [5]-[8]. Because of this, variable speed operation was introduced. In this context, the MPPT control is called to maximize the wind energy extraction. Various MPPT control models were based on the standard model [9], [10] which neglects the nonlinearity of the magnetic characteristic as well as the iron losses [11]-[14].

For these reasons, this article develops the principles of the high performance MPPT control for DFIG based on the optimization of the currents passed through the stator and rotor. Optimality is grasped in the context of maximizing torque and decreasing circulating currents [15]-[19]. The theoretical results are justified by the simulation which confirms that the developed controller has a certain robustness to disturbances. For some authors, the reference rotor flux is given the nominal value (or by defluxing). In such a case, the electromagnetic torque is close to its nominal value and the efficiency of the machine is maximum. But, in reality, the electromagnetic torque is not always fixed in a precise value and can have strong variations (depending on the mechanical torque applied) [20]-[23]. So, if the aerodynamic torque is small, there is

untapped stored energy in the stator and rotor inductances reducing the energy efficiency of the machine [24]-[26]. The article is structured as follows: the model of the wind turbine taking into account the nonlinear magnetic characteristic as well as the iron losses are described in section 2. The formulation of the problem, the design of the reference signals, and the development of an improved MPPT controller based on backstepping technique which exploited the magnetic characteristic nonlinearity are established in section 3. The robustness of the control law is presented by simulation in section 4, a conclusion is illustrated in section 5. At the end of the article, the list of references and the bibliography are presented.

2. WIND TURBINE MODEL IN PRESENCE OF NONLINEAR MAGNETIC CHARACTERISTIC AND IRON LOSSES

2.1. Turbine model

The aerodynamic wind power available at the blades is given by [19]:

$$P_{aero} = \frac{1}{2} \rho \pi R^2 C_p(\lambda, \beta) v_w^3 \tag{1}$$

with β is a blade pitch angle which will remain constant for our case study, $C_p(\lambda)$ is the coefficient of performance ($C_p(\lambda, \beta) \stackrel{\text{def}}{=} C_p(\lambda)$), R is the radius of the wind turbine rotor, ρ is the air density, v_w is the wind velocity and λ is the tip speed ratio, its expression is:

$$\lambda = \frac{R\omega_t}{v_w} \tag{2}$$

2.2. Nonlinear dynamic DFIG model

2.2.1. Iron losses

Generally, the iron losses of DFIG are most frequently modeled by of the equivalent iron loss resistance R_m associated in parallel with the magnetizing inductance X_j . although, in this paper, the proposed equivalent circuit of DFIG is inspired from [19], where the iron losses of DFIG are modeled by an equivalent resistance R_m associated at the same time in parallel with the stator cyclic leakage inductance $L_{s\sigma}$ and mutual cyclic inductance X_j . In fact, the simplicity and precision of the calculations of this technique justifies this choice [13], because, if we use the theorem of thevenin, we will obtain an equivalent circuit like that of the standard model (without iron losses). Figures 1(a) and (b) show the proposed equivalent circuit of the DFIG in the reference frame α and β respectively using concordia transformation. So, the iron resistance is a variable parameter which was identified experimentally on a 4 kW DFIG driven by a DC motor. The procedure described in [19] was used to determine the values of the iron loss resistance as well as the magnetizing reactance [22]. The iron resistance characteristic is shown in Figure 2.

From the Figure 1, the parameters R_s , R_m and $V_{s\alpha\beta}$ will be replaced by an equivalent voltage source $V_{sT\alpha\beta}$ in series with an equivalent resistance R_{sT} , from this, we are calculated in the stationary α - β reference frame the thevenin's equivalents parameters as [23]:

$$\begin{aligned} R_{sT} &= \frac{R_s R_m}{R_s + R_m}; V_{sT\alpha} = \frac{R_m}{R_s + R_m} V_{s\alpha}; V_{sT\beta} = \frac{R_m}{R_s + R_m} V_{s\beta}; \\ i_{sT\alpha} &= \frac{R_s + R_m}{R_m} i_{s\alpha} + \frac{V_{s\alpha}}{R_m}; i_{sT\beta} = \frac{R_s + R_m}{R_m} i_{s\beta} + \frac{V_{s\beta}}{R_m} \end{aligned} \tag{3}$$

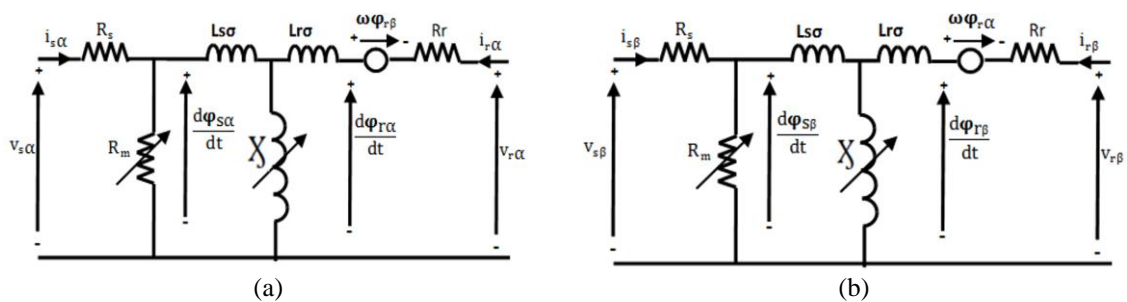


Figure 1. Proposed DFIG model in the ($\alpha\beta$) reference frame: (a) α –axis and (b) β –axis (iron loss resistance associated in parallel with the stator cyclic leakage inductance and mutual cyclic inductance)

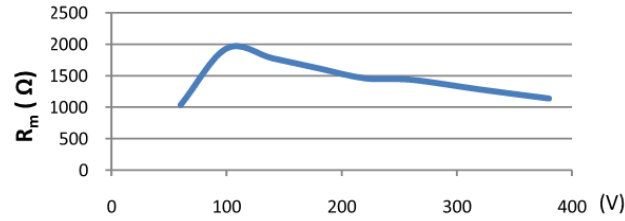


Figure 2. Experimental measurement of iron loss resistance equivalent characteristic

2.2.2. Nonlinear magnetic characteristic

We considered that the grid is stable and the stator flux aligned with the d axis. This gives:

$$v_{sq} = v_s, \varphi_{sq} = 0, \text{ and } \varphi_{sd} = \varphi_s \approx \frac{v_s}{\omega_s} \quad (4)$$

Therefore, the stator and rotor flux can be rewritten as:

$$\varphi_{sd} = \varphi_s = L_s i_{sTd} + X i_{rd} \quad (5)$$

$$\varphi_{sq} = 0 = L_s i_{sTq} + X i_{rq} \quad (6)$$

$$\varphi_{rd} = L_r i_{rd} + X i_{sTd} = L_r \sigma i_{rd} + X \frac{\varphi_s}{L_s} \quad (7)$$

$$\varphi_{rq} = L_r i_{rq} + X i_{sTq} = L_r \sigma i_{rq} \quad (8)$$

On the other hand, the stator and rotor currents contribute to the generation of the magnetizing flux along with the magnetizing current, denoted by:

$$i_\mu: i_{\mu d} = i_{sTd} + i_{rd}, i_{\mu q} = i_{sTq} + i_{rq} \quad (9)$$

$$\text{and we have } \varphi_{\mu d} = X i_{\mu d}, \varphi_{\mu q} = X i_{\mu q} \quad (10)$$

Where φ_μ is the magnetizing air-gap fluxes. In that case, the flux in (5), (6), (7) and (8) are given in the dq reference as [13]:

$$\varphi_s = l_{s\sigma} i_{sTd} + \varphi_{\mu d} \quad (11)$$

$$\varphi_{sq} = 0 = l_{s\sigma} i_{sTq} + \varphi_{\mu q} \quad (12)$$

$$\varphi_{rd} = l_{r\sigma} i_{rd} + \varphi_{\mu d} \quad (13)$$

$$\varphi_{rq} = l_{r\sigma} i_{rq} + \varphi_{\mu q} \quad (14)$$

The leakage inductances are grouped in the stator side, we pose l_{seq} is the equivalent inductance to the stator side of both the stator and the rotor leakage brought, that gives $l_{r\sigma} = 0$ and $l_{s\sigma} = l_{seq}$. Next, the inductances L_s and L_r can be rewritten like that:

$$L_s = l_{seq} + X \text{ and } L_r = l_{r\sigma} + X = X \quad (15)$$

Figure 3(a) give the variations of mutual inductance as a function of the corresponding magnetizing current. We suppose that the magnetizing flux direction remains unchanged and that it saturates only in amplitude, which allowed us to admit that φ_μ and i_μ are in phase. Figure 3(b) shows the magnetic characteristic $\Phi_\mu = \lambda(I_\mu)$ where Φ_μ and I_μ are the norms values. Of the above, the instantaneous values φ_μ and i_μ are given by:

$$\varphi_{\mu} = \frac{\Phi_{\mu}}{I_{\mu}} i_{\mu} \tag{16}$$

In the following, we pronounce the static magnetization parameter χ , defined as [23]:

$$\chi = \frac{\Phi_{\mu}}{I_{\mu}} \tag{17}$$

First, we note some experimental points of the DFIG magnetic characteristic to make the approximation of the mutual inductance $\chi(I_{\mu})$. Then, we can easily deduce the magnetizing flux norm Φ_{μ} (with $\Phi_{\mu} = \Phi_r$) in function of the magnetizing current I_{μ} .

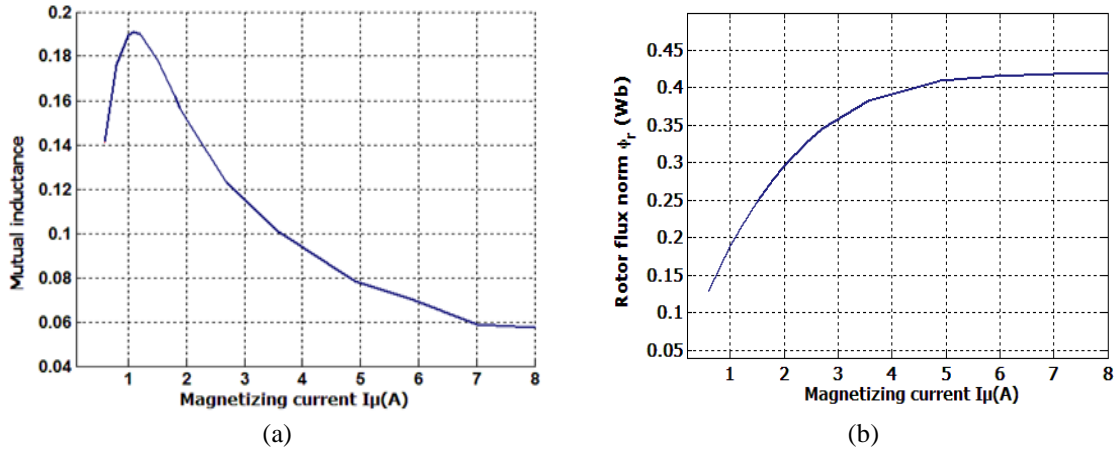


Figure 3. Experimental measurement of DFIG: (a) magnetizing inductance and (b) nonlinear magnetic characteristic

2.2.3. Improved model of DFIG

From the above and taking into account the iron losses and the nonlinearity of the magnetic saturation, the improved model of DFIG can be rewritten in the dq reference frame as follows:

$$\begin{cases} \dot{x} = f(x, u, y) \stackrel{\text{def}}{=} [f_1(x, u, y) \ f_2(x, u, y) \ \dots \ f_5(x, u, y)]^T \\ h(x) \stackrel{\text{def}}{=} [h_1(x) \ h_2(x) \ h_3(x)]^T \end{cases} \tag{18}$$

with

$$x = [x_1 \ x_2 \ x_3 \ x_4 \ x_5]^T = [i_{sTd} \ i_{sTq} \ \varphi_{rd} \ \varphi_{rq} \ \Omega]^T$$

$$u = [v_{sTd} \ v_{sTq}]^T; \ y = [v_{rd} \ v_{rq}]^T$$

$$\begin{bmatrix} f_1 \\ f_2 \\ f_3 \\ f_4 \\ f_5 \end{bmatrix} = \begin{bmatrix} -\eta i_{sTd} + \omega_s i_{sTq} + \Gamma \varphi_{rq} + \frac{1}{l_{seq}} \omega \varphi_{rq} + \frac{1}{l_{seq}} v_{sTd} - \frac{1}{l_{seq}} v_{rd} \\ -\omega_s i_{sTd} - \eta i_{sTq} - \frac{1}{l_{seq}} \omega \varphi_{rd} + \Gamma \varphi_{rq} + \frac{1}{l_{seq}} v_{sTq} - \frac{1}{l_{seq}} v_{rq} \\ R_r i_{sTd} - l_{seq} \Gamma \varphi_{rd} + g \omega_s \varphi_{rq} + v_{rd} \\ R_r i_{sTq} - g \omega_s \varphi_{rd} - l_{seq} \Gamma \varphi_{rq} + v_{rq} \\ \frac{\mu}{J} (\varphi_{sq} i_{rd} - \varphi_{sd} i_{rq}) - \frac{f}{J} \Omega + \frac{T_{mec}}{J} \end{bmatrix} \tag{19}$$

Where: $l_{seq} = \sigma L_s$; $\sigma = 1 - \frac{\chi^2}{L_r L_s}$; $\eta = \frac{R_r + R_s T}{l_{seq}}$; $\Gamma = \frac{R_r}{l_{seq} \chi}$; $\mu = \frac{\sigma P R_r}{l_{seq} 2 \Gamma}$. With: J : total inertia constant ; f : viscous friction coefficient; (φ_s, φ_r) : stator , rotor flux components; Ω : DFIG rotor speed; (R_s, R_r) : stator and rotor resistances.

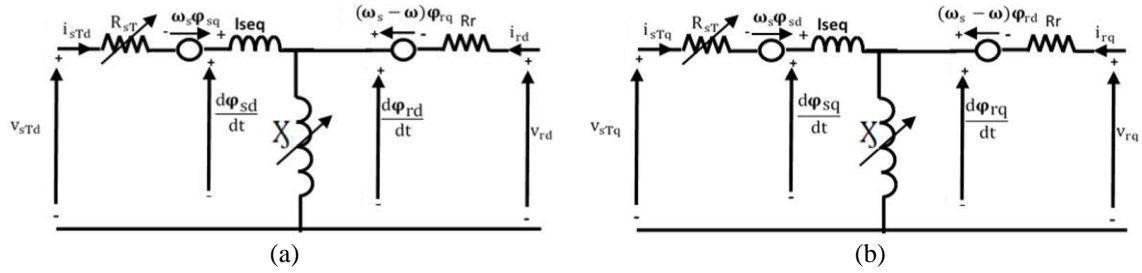


Figure 4. Proposed DFIG equivalent circuit accounting the iron losses and the nonlinearity of the magnetic saturation: (a) d axis and (b) q axis

Figures 4(a) and 4(b) show the proposed circuit of the DFIG taking into account the iron losses and the nonlinearity of the magnetic saturation in the reference frame d and q respectively using Park transformation. In the above model, the parameter Γ is the unique parameter that varies in function of magnetic state of the DFIG, this relation has been given a polynomial approximation [24]-[26], i.e.:

$$\Gamma = K(\Phi_r), \text{ with } : K(\Phi_r) = a_0 + a_1\Phi_r + a_2\Phi_r^2 + \dots + a_n\Phi_r^n$$

The a_i 's are constant coefficients, identified with polyfit MATLAB function. So, the magnetic characteristic of the DFIG is denoted $\Phi_r = \gamma(I_\mu)$ where I_μ denotes the norm of the magnetizing current and $\Phi_r = \Phi_\mu$. From the experimental points (I_μ, Φ_μ) , we deduce a polynomial function approximation of the characteristic (Φ_r, Γ) as depicted Figure 5. The parameter values of DFIG used in experimental tests are given in Table 1.

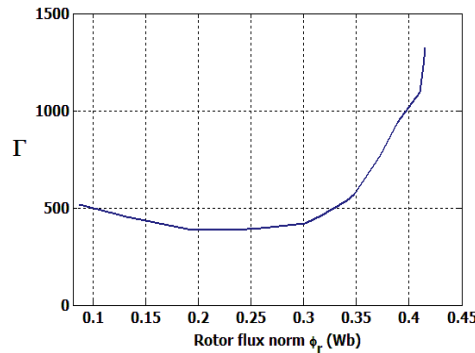


Figure 5. The characteristic (Φ_r, Γ)

Table 1. Parameters of DFIG 4 kW

Characteristic	Value
Stator resistance	1.25 Ω
Rotor resistance	0.17 Ω
Mutual inductance	0.0772 H
Rotor leakage inductance	0.0018 H
Stator leakage inductance	0.00096 H
Generator inertia	0.33 kg m ²
Viscous friction coefficient	0.001 m/s

3. REFERENCE ROTOR FLUX CONSTRUCTION AND THE ENHANCED OPTIMAL CONTROL

The present section presents a new and optimal approach that properly accounts for the nonlinear magnetic characteristic to control DFIG. Notice that in previous works, the standard model can be referred to linear model (LM), from the nonlinear model (NLM), and this while keeping the parameter Γ constant. Thus, we describe a new control strategy based on a method for optimizing the rotor flux reference to minimize stator

and rotor current absorbed [23]-[26]. the performance of this optimization law is validated by means of simulation.

3.1. Problem formulation

The problem of controlling variable speed wind turbines is addressed. The majority of previous works considered that the reference of the reactive power of the stator was null and the magnetic characteristic was linear. However, the machine operation mode is not optimal of the large electromagnetic torque with $Q_s=0$. In the present section, we will develop a new optimal MPPT control strategy taking into account the nonlinearities of the machine (in order to lower the total currents consumption in both the stator and rotor).

The control objective is to follow the maximum of the wind power captured and to minimize the currents transited by generating an optimal rotor flux in line. In this context, the rotor flux norm Φ_r must track perfectly the flux reference $\Phi_{r-ref} = H(I_r, I_s)$, where (I_r, I_s) are the rotor and stator currents norms and the function H will be resolute in order that $\Phi_r = \Phi_{r-ref}$ involve the minimization of the stator and rotor currents circulated in the induction machine for getting a maximum electromagnetic torque [23]-[26].

3.2. Optimal rotor flux reference

Firstly, we find a relation between the rotor flux, stator and rotor currents norms. In this respect, one considers the DFIG model developed in (19); thus, the stator and rotor currents can be rewritten by:

$$i_{rd} = \frac{L_s \varphi_{rd} - X \varphi_s}{\sigma L_s L_r} = \frac{\varphi_{rd}}{\sigma X} - \frac{\varphi_s}{l_{seq}}, i_{rq} = \frac{\varphi_{rq}}{X \sigma} \quad (20)$$

$$i_{sTd} = \frac{\varphi_s - \varphi_{rd}}{l_{seq}}, i_{sTq} = -\frac{X}{L_s} i_{rq} \quad (21)$$

On the other hand, the rotor flux can be rewritten as:

$$\varphi_{rd}^2 = X^2 (i_{sTd}^2 + i_{rd}^2 + 2i_{sTd}i_{rd}), \varphi_{rq}^2 = X^2 (i_{sTq}^2 + i_{rq}^2 + 2i_{sTq}i_{rq}) \quad (22)$$

Then, using (20) and (21), we'll have:

$$i_{sTd}i_{rd} = \frac{\varphi_s \varphi_{rd}}{\sigma L_r l_{seq}} - \frac{\varphi_{rd}^2}{\sigma L_r l_{seq}} - \frac{\varphi_s^2}{l_{seq}^2} + \frac{\varphi_s \varphi_{rd}}{l_{seq}^2} = \varphi_s \varphi_{rd} \left(\frac{1}{l_{seq}^2} + \frac{1}{\sigma L_r l_{seq}} \right) - \frac{\varphi_{rd}^2}{\sigma L_r l_{seq}} + \frac{\varphi_{rd}^2}{\sigma L_r l_{seq}} - \frac{\varphi_{sd}^2}{l_{seq}^2} \quad (23)$$

$$i_{sTq}i_{rq} = -\frac{\varphi_{rd}^2}{\sigma L_r l_{seq}} \quad (24)$$

Accordingly, one has:

$$\Phi_r^2 = X^2 (I_s^2 + I_r^2 + 2(i_{sTd}i_{rd} + i_{sTq}i_{rq})) \quad (25)$$

We replace $i_{sd}i_{rd}$, and $i_{sq}i_{rq}$ by their expressions according to (23)-(24), we are the expressions of rotor flux norm in function to the stator and rotor currents norms:

$$\varphi_r^2 = X^2 (I_s^2 + I_r^2) + 2X^2 \left(\frac{1}{l_{seq}^2} + \frac{1}{\sigma L_r l_{seq}} \right) (\varphi_{sd} \varphi_{rd} + \varphi_{sq} \varphi_{rq}) - 2X^2 \frac{\varphi_{rd}^2}{\sigma L_r l_{seq}} - 2X^2 \frac{\varphi_s^2}{l_{seq}^2} \quad (26)$$

The electromagnetic torque T_{em} can be written by:

$$T_{em} = \frac{p(\varphi_{sd} \varphi_{rq} - \varphi_{sq} \varphi_{rd})}{l_{seq}} \quad (27)$$

Then, (26) can be simplified to:

$$\left(\frac{1}{X^2} + \frac{2}{\sigma X l_{seq}} \right) \varphi_r^2 - (I_s^2 + I_r^2) + \frac{2\varphi_s^2}{l_{seq}^2} - \left(\varphi_s^2 - \frac{l_{seq} V_{sq}}{R_s} \sqrt{\varphi_s^2 - \left[\frac{R_s T_{em}}{p V_{sq}} + \frac{w_s \varphi_s^2}{V_s} \right]^2} \right) \left(\frac{2}{l_{seq}^2} + \frac{2}{\sigma L_r l_{seq}} \right) = 0 \quad (28)$$

Figure 6 shows the curves representing the sum of the squares of the current modules ($I_s^2 + I_r^2$) versus the flux Φ_r , for various values of the electromagnetic torque T_{em} . At present, it is easy to observe that, for each value of the sum ($I_s^2 + I_r^2$), there are several different operating points by the value of rotor flux norm Φ_r and T_{em} . For example, a torque $T_{em} = 5\text{Nm}$ can be produced, for the generator 4kw (Table 1), with:

- A current $I_s^2 + I_r^2 = 490$ A and a flux $\Phi_r = 0.2$ Wb;
- A current $I_s^2 + I_r^2 = 20$ A and a flux $\Phi_r = 0.40$ Wb;

The best operation point from an energetic viewpoint, is the one which corresponds to the minimum of currents circulations. From Figure 6, it is usually seen that there is a unique couple $(\Phi_r, (I_s^2 + I_r^2))$ for any T_{em} , which engages the least possible values of the stator and rotor currents. For our case study $\Phi_{r-ref} = 0.4\text{Wb}$.

The stator active and reactive powers are given by:

$$P_s = v_{sTd} i_{sTd} + v_{sTq} i_{sTq} \quad (29)$$

and

$$Q_s = v_{sTq} i_{sTd} - v_{sTd} i_{sTq} \quad (30)$$

For $v_{sTq} = V_s$ and $v_{sTd} = 0$, (29) and (30) become:

$$P_s = V_s i_{sTq} \quad (31)$$

and

$$Q_s = V_s i_{sTd} \quad (32)$$

Introducing (20) and (21) into (31) and (32), we obtain:

$$P_s = -\frac{V_s X}{L_s} i_{rq} \quad (33)$$

and

$$Q_s = V_s \frac{\varphi_s}{L_s} - V_s \frac{X}{L_s} i_{rd} \quad (34)$$

Indeed using (33)-(34) and (20)-(21), we can deduce the expression of the rotor flux magnitude reference ($\Phi_{ref} = \sqrt{\varphi_{rd}^2 + \varphi_{rq}^2}$) according to Q_{s-ref} (stator reactive power reference)

$$\Phi_{ref}^2 = \left[\varphi_s - \frac{l_{seq}}{V_s} Q_{s-ref} \right]^2 + \left[\frac{l_{seq}}{V_s} P_s \right]^2 \quad (35)$$

The stator flux φ_s is assumed constant (the grid is considered stable).

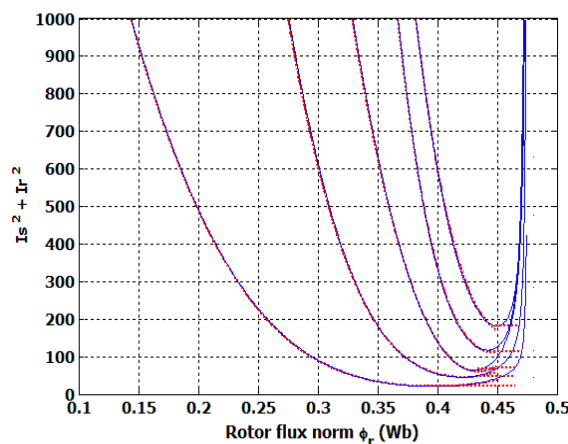


Figure 6. Sum of the squares of the current modules ($I_s^2 + I_r^2$) as versus rotor flux Φ_r for different T_{em} values

3.3. Improved MPPT control

The main objective of the control strategy is to develop an optimal control law in order to optimize the different operations points of the wind turbine [13]. For this, an enhanced backstepping controller has been designed to force the system to track their references (Ω_{ref} , Φ_{r-ref}) where Ω_{ref} is the optimal rotor speed reference illustrated in Figure 7 and Φ_{r-ref} is the rotor flux reference (35).

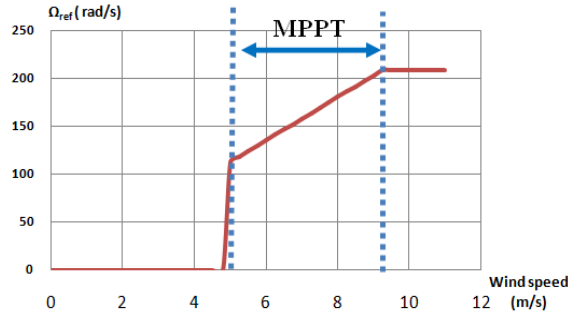


Figure 7. Optimal rotor speed reference in function the speed wind [13]

For reasons of simplification (backstepping control of the rotor flux in only one step), the control of the rotor flux will be assured by controlling the stator reactive power described by (34). Firstly, we consider the following errors:

$$e_1 = \Omega_{ref} - \Omega \quad (36)$$

$$e_3 = Q_{s_ref} - Q_s \quad (37)$$

Step 1. It follows from (19), (33), (34), (36) and (37) that the dynamics errors e_1 and e_3 are:

$$\dot{e}_1 = \dot{\Omega}_{ref} - \dot{\Omega} = \dot{\Omega}_{ref} + \frac{\mu}{J} \varphi_{sd} i_{rq} + \frac{f}{J} \Omega - \frac{T_{mec}}{J} \quad (38)$$

$$\dot{e}_3 = \dot{Q}_{s_ref} - \dot{Q}_s = \dot{Q}_{s_ref} + V_s \frac{R_s}{L_s \omega_s} \frac{d}{dt} i_{sq} + V_s \frac{X}{L_s} \frac{d}{dt} i_{rd} \quad (39)$$

$$\dot{e}_3 = \dot{Q}_{s_ref} - V_s \frac{X R_s}{L_s^2 \omega_s} \frac{d}{dt} i_{rq} + V_s \frac{X}{L_s} \frac{d}{dt} i_{rd} \quad (40)$$

Indeed, considering the function Lyapunov candidate:

$$V_1 = \frac{1}{2} e_1^2 + \frac{1}{2} e_3^2 \quad (41)$$

We deduce that:

$$\dot{V}_1 = e_1 \dot{e}_1 + e_3 \dot{e}_3 = -k_1 e_1^2 - k_3 e_3^2 \quad (42)$$

Where k_1 and k_3 are positive real parameters to be chosen as described in [13]. On the other hand, in (38), $\varphi_{sd} i_{rq}$ is considered as a virtual control signal which will temporarily be like the real control signal, the error in (38) assures the global asymptotic stability, letting:

$$\left(\varphi_{sd} i_{rq} \right)_{ref} = \mu_1 \text{ with: } \mu_1 \stackrel{\text{def}}{=} \frac{J}{\mu} \left(-\dot{\Omega}_{ref} - \frac{f}{J} \Omega + \frac{T_{mec}}{J} - k_1 e_1 \right) \quad (43)$$

As the quantity $\varphi_{sd} i_{rq}$ can't be equal to μ_1 because isn't actual control signal. Indeed, we take the stabilizing function μ_1 in the first. Step 2. Now introduce the new error:

$$e_2 = \mu_1 - \varphi_{sd} i_{rq} \quad (44)$$

Then, the dynamic of the error e_1 are given as:

$$\dot{e}_1 = -k_1 e_1 - \frac{\mu}{J} e_2 \quad (45)$$

So, the time derivative of the function V_1 is:

$$\dot{V}_1 = -k_1 e_1^2 - k_3 e_3^2 - \frac{\mu}{J} e_1 e_2 \quad (46)$$

The actual control signals V_{rd} and V_{rq} are choosing so that all errors (e_1, e_2, e_3) converge to zero:

$$\dot{e}_2 = \dot{\mu}_1 - \varphi_{sd} \frac{d}{dt} i_{rq} \quad (47)$$

$$\text{and } \dot{e}_2 = \frac{J}{\mu} \left(-\ddot{\Omega}_{ref} - \frac{f}{J} \dot{\Omega} + \frac{\dot{T}_{mec}}{J} - k_1 \dot{e}_1 \right) - \varphi_{sd} \frac{d}{dt} i_{rq} \quad (48)$$

From (3) and (4), we can write:

$$\frac{d}{dt} i_{rd} = \frac{1}{L_r \sigma} (V_{rd} - R_r i_{rd} - \frac{\chi}{L_s} \frac{d\varphi_s}{dt} + L_r \sigma \omega_r i_{rq}) \quad (49)$$

$$\frac{d}{dt} i_{rq} = \frac{1}{L_r \sigma} (V_{rq} - R_r i_{rq} - L_r \sigma \omega_r i_{rd} - \frac{\chi}{L_s} \omega_r \varphi_s) \quad (50)$$

Introducing (25) and (26) in (27) and (24), we obtain:

$$\dot{e}_2 = \frac{J}{\mu} \left(-\ddot{\Omega}_{ref} - \frac{f}{J} \dot{\Omega} + \frac{\dot{T}_{mec}}{J} + k_1^2 e_1 \right) + k_1 e_2 - \frac{\varphi_{sd}}{L_r \sigma} (V_{rq} - R_r i_{rq} - L_r \sigma \omega_r i_{rd} - \frac{\chi}{L_s} \omega_r \varphi_s)$$

This can be condensed as:

$$\dot{e}_2 = \mu_2 - \frac{\varphi_{sd} V_{rq}}{L_r \sigma} \quad (51)$$

With $\mu_2 = \frac{J}{\mu} \left(-\ddot{\Omega}_{ref} - \frac{f}{J} \dot{\Omega} + \frac{\dot{T}_{mec}}{J} + k_1^2 e_1 \right) + k_1 e_2 - \frac{\varphi_{sd}}{L_r \sigma} (-R_r i_{rq} - L_r \sigma \omega_r i_{rd} - \frac{\chi}{L_s} \omega_r \varphi_s)$

$$\text{and } \dot{e}_3 = \dot{Q}_{s_ref} - V_s \frac{\chi R_s V_{rq}}{L_s^2 L_r \sigma \omega_s} + \frac{\chi R_s V_s}{L_s^2 L_r \sigma \omega_s} \left(R_r i_{rq} + L_r \sigma \omega_r i_{rd} + \frac{\chi}{L_s} \omega_r \varphi_s \right) + \frac{\chi V_s}{L_s L_r \sigma} V_{rd} + \frac{\chi V_s}{L_s L_r \sigma} \left(-R_r i_{rd} - \frac{\chi}{L_s} \frac{d\varphi_s}{dt} + L_r \sigma \omega_r i_{rq} \right) \quad (52)$$

Then, let us consider the Lyapunov function candidate as:

$$V_2 = \frac{1}{2} e_1^2 + \frac{1}{2} e_2^2 + \frac{1}{2} e_3^2 \quad (53)$$

The control signals V_{rq} and V_{rd} can be deduced from (51) and (52) satisfying $\dot{V}_2 < 0$:

$$V_{rq} = \frac{L_r \sigma}{\varphi_s} (k_2 e_2 + \mu_2) \quad (54)$$

$$V_{rd} = \frac{L_s L_r \sigma}{V_s \chi} \left[-k_3 e_3 - \dot{Q}_{s_ref} + V_s \frac{\chi R_s V_{rq}}{L_s^2 L_r \sigma \omega_s} - \sigma \omega_r i_{rd} + \frac{\chi}{L_s} \omega_r \varphi_s \right] + R_r i_{rd} + \frac{\chi}{L_s} \frac{d\varphi_s}{dt} - L_r \sigma \omega_r i_{rq} \quad (55)$$

Where k_2 is a new positive constant. In fact by substituting (54) and (55) in (53), the time derivative of (53):

$$\dot{V} = -k_1 e_1^2 - k_2 e_2^2 - k_3 e_3^2 < 0 \quad (56)$$

Which ensures the global asymptotic stability of the system.

4. SIMULATIONS RESULTS

In this section, we will present the importance of the new control strategy (non-linear model with optimal flux NLMOF), introducing the optimal rotor flux reference illustrated by Figure 8, compared to the control strategies using the constant rotor flux reference (case of the linear model with constant flux LMCF or nonlinear model with constant flux NLMCF). The comparison is performed using DFIG and Turbine parameters considered in Tables 1 and 2.

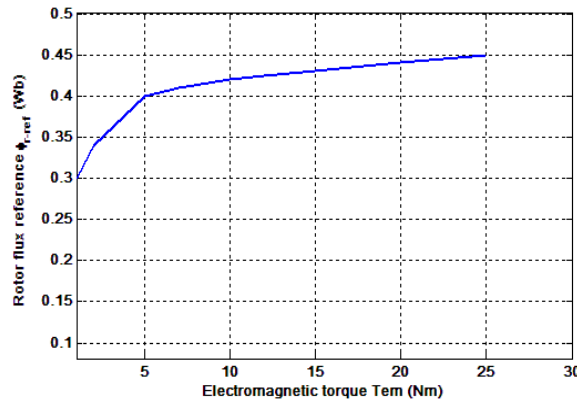


Figure 8. Characteristic of the rotor flux reference obtained by interpolating the points (T_{em}, Φ_{r-ref})

Table 2. Turbine parameters

Characteristic	Value
Turbine radius, R	3m
Gear box ratio	1:8.5
Rated wind speed	10.5 m/s
Number of blades	3
Power	5 kW
Rotor inertia	0.05 kg m ²
Cut-in wind speed	4.25 m/s

4.1. Hegemony of the NLMOF strategy over the LMCF strategy

The simulation protocol is designed in order to test the performance of the HP-MPPT controller (used the NLMOF) operating under different conditions by considering two steps of the wind speed (Figure 9) and load torque (Figure 10). Recall that the NLMOF regulator involves the optimal flux reference depicted in Figure 8. The HP-MPPT control laws defined by (54) and (55) receives the following design parameter values, which have proven to be practical: $k_1 = 1000$, $k_2 = 300$ and $k_3 = 50$.

The optimal specific speed 8,1 with MPPT control are presented in Figure 11. The dynamic responses of the optimal flux NLMOF and constant flux LMCF regulator are presented in Figure 12. The control of rotor flux with the NLMOF and LMCF strategies are presented in Figures 13 and 14 respectively. According to the results obtained in Figure 15, it is confirmed that under all operating conditions, the NLMOF regulator requires smaller current than the constant flux reference regulator LMCF. Figure 16 confirms the performance of our regulator by the pace of joule effect losses for LMCF and NLMOF strategies. The active stator and rotor power are presented in Figures 17 and 18 respectively for LMCF and NLMOF regulators. The dynamic and the performance under different operating parameter changes of the proposed regulator have been affirmed further by Figures 19 and 20 which presented the reactive stator and rotor power respectively for LMCF and NLMOF controllers.

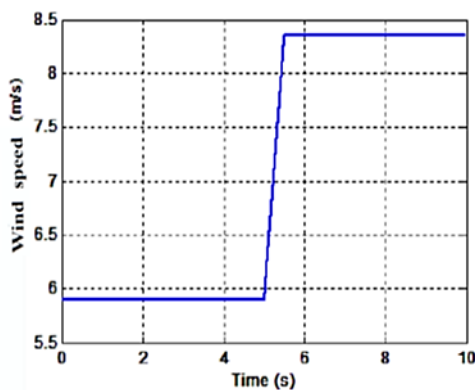


Figure 9. Wind speed

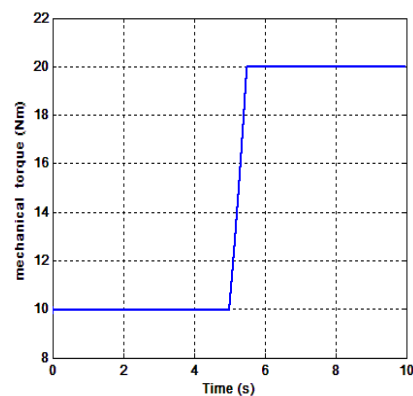


Figure 10. Load torque applied

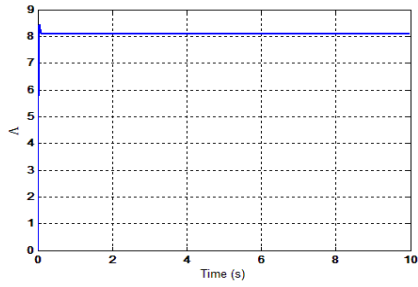


Figure 11. Optimal specific speed with MPPT control

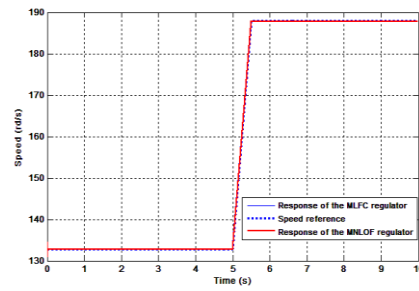


Figure 12. The Speed reference (to ensure MPPT), the responses of the optimal flux NLMOF and constant flux LMCF regulator

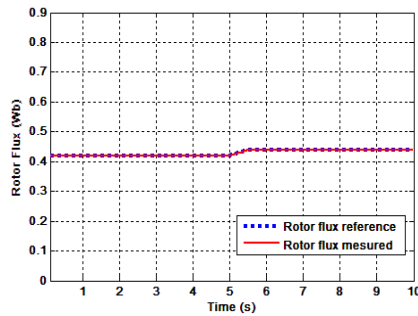


Figure 13. Regulation of rotor flux with the NLMOF strategy (The online flow reference generated (T_{em}, Φ_{r-ref})).

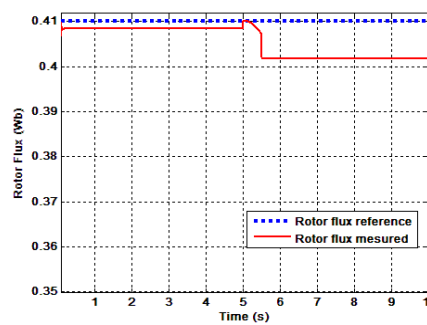


Figure 14. Regulating the rotor flux with the LMCF control strategy (which imposes a constant flux reference)

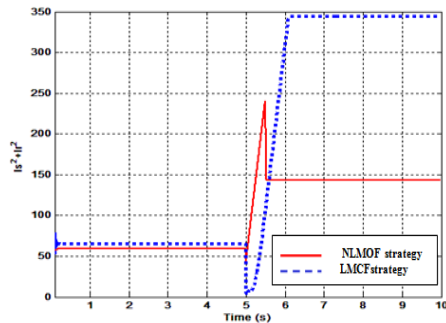


Figure 15. Sum of squares of norm ($I_s^2 + I_r^2$) for LMCF and NLMOF regulators

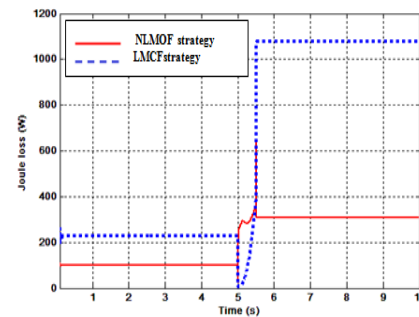


Figure 16. Joule effect losses for LMCF and NLMOF regulators

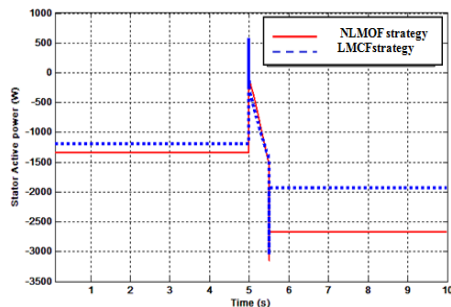


Figure 17. Active stator power (W) for LMCF and NLMOF regulators

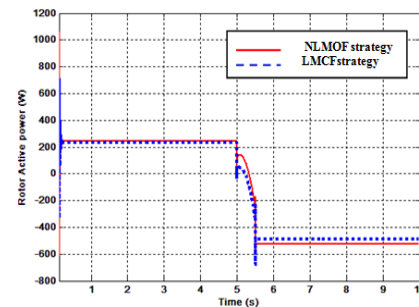


Figure 18. Active rotor power (W) for LMCF and NLMOF regulators

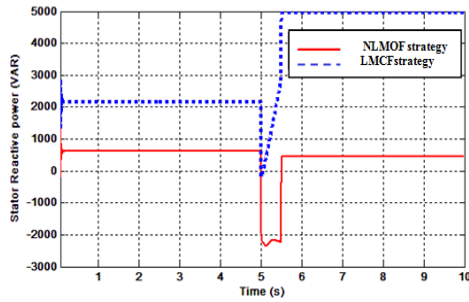


Figure 19. Reactive stator power (VAR) for LMOF and NLMOF regulators

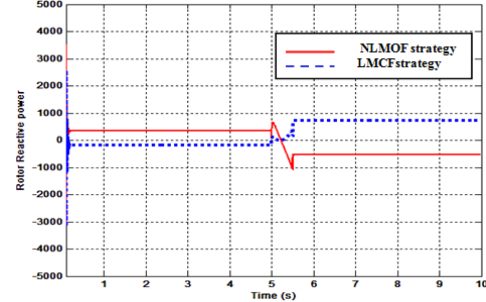


Figure 20. Reactive rotor power (VAR) for LMOF and NLMOF regulators

4.2. Hegemony of the NLMOF strategy over the LMOF strategy

The simulation protocol is similar to part 4.1 (Figures 9 and 10). Recall that the NLMOF regulator is defined for (19) in combination with the optimal flux generator (shown in Figure 8). So to have the LMOF regulator, it is sufficient to make the following changes in (19):

- The parameter Γ in (19) is held constant, equal to $\hat{\Gamma} \approx 460 \Omega H^{-1}$.
- The rotor flux reference is given by the signal depicted in Figure 8.
- The controller parameters are set to the following values: $k_1 = 1000, k_2 = 300$ and $k_3 = 50$.

Figure 21 shows that the Sum of squares norm ($I_s^2 + I_r^2$) is lower with the NLMOF regulator. Figure 22 shows the quality of flux tracking obtained with the NLMOF and LMOF control strategies. So, Figure 23 presents the active stator power for LMOF and NLMOF regulators. Also, from the energy point of view, is also illustrated by Figure 24 when the rotor power produced by NLMOF regulator is more than LMOF regulator.

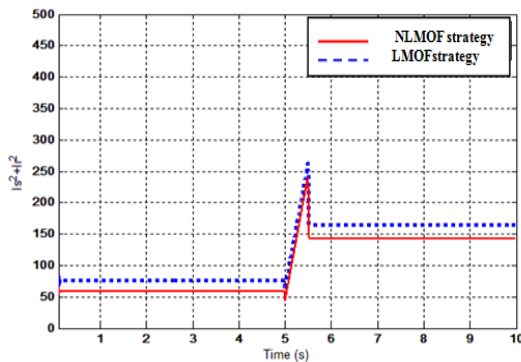


Figure 21. Sum of squares norm ($I_s^2 + I_r^2$) for LMOF and NLMOF regulators

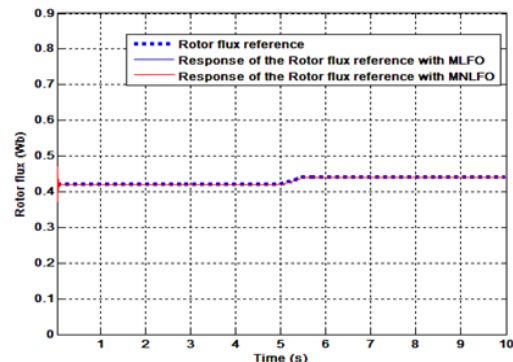


Figure 22. Regulating of rotor flux for LMOF and NLMOF regulators

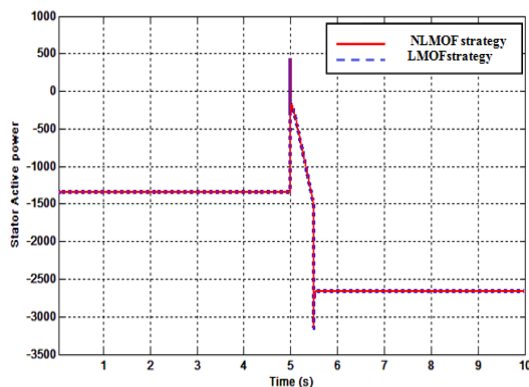


Figure 23. Active stator power (W) for LMOF and NLMOF regulators

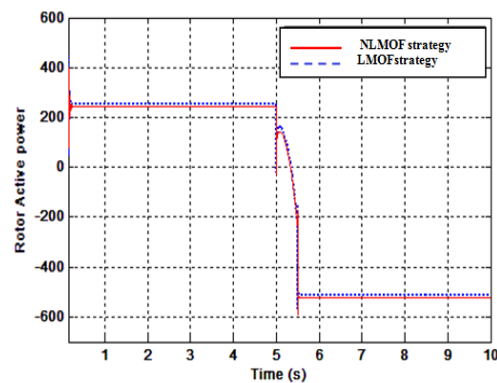


Figure 24. Active rotor power (W) for LMOF and NLMOF regulators

5. CONCLUSION

The problem of controlling the DFIG in the presence of nonlinear saturation magnetic state are evoked. A new speed and rotor flux regulator has been developed using the optimal backstepping approach to optimize the currents circulated in the machine. Also, the proposed regulator comprises a reference rotor flux generator dependent on the nonlinear magnetic state. In addition, it is demonstrated by simulation that, under all operating conditions, that the current transited is really lower with the regulator NLMOF. The performance of the proposed control laws has been demonstrated by simulation studies performed in the MATLAB/Simulink® environment.

REFERENCES

- [1] S. Hu, X. Lin, Y. Kang and X. Zou, "An Improved Low-Voltage Ride-Through Control Strategy of Doubly Fed Induction Generator During Grid Faults," *IEEE Transactions on Power Electronics*, vol. 26, no. 12, pp. 3653-3665, 2011, doi: 10.1109/TPEL.2011.2161776.
- [2] J. Liang, W. Qiao and R. G. Harley, "Feed-Forward Transient Current Control for Low-Voltage Ride-Through Enhancement of DFIG Wind Turbines," *IEEE Transactions on Energy Conversion*, vol. 25, no. 3, pp. 836-843, Sept. 2010, doi: 10.1109/TEC.2010.2048033.
- [3] E. Tremblay, S. Atayde and A. Chandra, "Comparative Study of Control Strategies for the Doubly Fed Induction Generator in Wind Energy Conversion Systems: A DSP-Based Implementation Approach," *IEEE Transactions on Sustainable Energy*, vol. 2, no. 3, pp. 288-299, 2011, doi: 10.1109/TSTE.2011.2113381.
- [4] X. Xiao, R. Yang, Z. Zheng and Y. Wang, "Cooperative Rotor-Side SMES and Transient Control for Improving the LVRT Capability of Grid-Connected DFIG-Based Wind Farm," *IEEE Transactions on Applied Superconductivity*, vol. 29, no. 2, pp. 1-5, 2019, doi: 10.1109/TASC.2018.2881315.
- [5] F. K. A. Lima, A. Luna, P. Rodriguez, E. H. Watanabe and F. Blaabjerg, "Rotor Voltage Dynamics in the Doubly Fed Induction Generator During Grid Faults," *IEEE Transactions on Power Electronics*, vol. 25, no. 1, pp. 118-130, 2010, doi: 10.1109/TPEL.2009.2025651.
- [6] B. Beltran, T. Ahmed-Ali and M. E. H. Benbouzid, "Sliding Mode Power Control of Variable-Speed Wind Energy Conversion Systems," *IEEE Transactions on Energy Conversion*, vol. 23, no. 2, pp. 551-558, 2008, doi: 10.1109/TEC.2007.914163.
- [7] S. E. Rhaili, A. Abbou, S. Marhraoui, R. Moutchou, N. El Hichami, "Robust Sliding Mode Control with Five Sliding Surfaces of Five-Phase PMSG Based Variable Speed Wind Energy Conversion System," *International Journal of Intelligent Engineering and Systems*, vol. 13, no. 4, pp. 346-357, 2020, doi: 10.22266/ijies2020.0831.30.
- [8] M. Alizadeh and S. S. Kojor, "Augmenting effectiveness of control loops of a PMSG (permanent magnet synchronous generator) based wind energy conversion system by a virtually adaptive PI (proportional integral) controller," *Energy*, vol. 91, pp. 610-629, 2015, doi: 10.1016/j.energy.2015.08.047.
- [9] S. Ganjefar and A. A. Ghasemi, "A novel-strategy controller design for maximum power extraction in stand-alone windmill systems," *Energy*, vol. 76, pp. 326-335, 2014, doi: 10.1016/j.energy.2014.08.024.
- [10] A. F. Zohra, B. I. Khalil, L. Slimane, S. Youcef, and M. Benyounes, "Artificial intelligence control applied in wind energy conversion system," *International Journal of Power Electronics and Drive Systems*, vol. 9, no. 2, pp. 571-578, 2018, doi: 10.11591/ijpeds.v9.i2.pp571-578, 2018.
- [11] I. Yasmine, E. B. Chakib, B. Badre, "Power control of DFIG-generators for wind turbines variable-speed," *International Journal of Power Electronics and Drive Systems*, vol. 8, no. 1, pp. 444-453, 2017, doi: 10.11591/ijpeds.v8.i1.pp444-453.
- [12] S. Kail, A. Bekri and A. Hazzab "Study of automatic generation control in two area power system with DFIG-based wind energy conversion," *International Journal of Power Electronics and Drive Systems*, vol. 10, no. 4, pp. 20118-2125, 2019, doi: 10.11591/ijpeds.v10.i4.pp2118-2125, <https://ijpeds.iaescore.com/index.php/IJPEDS/article/view/21429>.
- [13] Y. Majdoub, A. Abbou, M. Akherraz and R. El akhrif, "Intelligent Backstepping Control of Variable Speed DFIG-Wind Turbine under unbalanced grid voltage conditions using Genetic Algorithm optimization," *International Review of Electrical Engineering*, vol. 10, no. 6, pp. 716-726, 2015, doi: 10.15866/iree.v10i6.7530.
- [14] Y. Majdoub, A. Abbou and M. Akherraz, "Variable speed control of DFIG-wind turbine with wind estimation," *International Renewable and Sustainable Energy Conference (IRSEC)*, 2014, pp. 268-274, doi: 10.1109/IRSEC.2014.7059879.
- [15] G. Lefebvre, V. L. Digarcher, J. Y. Gauthier, A. Hijazi and X. L. Shi, "Electrical parameter observation for induction machine sensorless drive using a sensitivity and observability based EKF," *IEEE International Power Electronics and Motion Control Conference (PEMCC)*, 2016, pp. 806-811, doi: 10.1109/EPEPEMCC.2016.7752097.
- [16] Y. Zhou, P. Bauer, J. A. Ferreira and J. Pierik, "Operation of Grid-Connected DFIG Under Unbalanced Grid Voltage Condition," *IEEE Transactions on Energy Conversion*, vol. 24, no. 1, pp. 240-246, 2009, doi: 10.1109/TEC.2008.2011833.
- [17] M. J. Zandzadeh, and A. Vehadi, "Modeling and improvement of direct power control of DFIG under unbalanced grid voltage condition," *Electrical Power and Energy Systems*, vol. 59, pp. 58-65, 2014, doi: 10.1016/j.ijepes.2014.01.022.
- [18] M. Bašić, D. Vukadinović and G. Petrović, "Dynamic and pole-zero analysis of self-excited induction generator using a novel model with iron losses," *International Journal of Electrical Power & Energy Systems*, vol. 42, no. 1, pp. 105-118, 2012, doi: 10.1016/j.ijepes.2012.03.003.
- [19] I. Boldea and SA. Nasar, "The induction machine handbook," *CRC Press*; 2002.
- [20] R. E. Akhrif, A. Abbou, M. Barara, M. Akherraz and Y. Majdoub, "dSPACE Implementation for a Fuzzy Logic Voltage Control using a Self-Excited Induction Generator and a Voltage Source Inverter," *International Journal of Electrical and Computer Engineering*; vol. 7, no. 4, pp. 1749-1759, 2017, doi: 10.1177/0309524X18791384.
- [21] A. M. Sylla and M. L. Doumbia, "Maximum power control of grid-connected DFIG-based wind systems" *IEEE Electrical Power and Energy Conference*, 2012, pp. 267-273, doi: 10.1109/EPEC.2012.6474963.
- [22] Y. Majdoub, A. Abbou, M. Akherraz, R. E. Akhrif, "Design of an improved MPPT control of DFIG Wind Turbine under unbalanced grid voltage using a flux sliding mode observer," *IJPEDS International Journal of Power Electronics and Drive Systems*, vol. 8, no. 4, pp. 1723-1731, 2017, doi: 10.11591/ijpeds.v8.i4.pp1723-1731.
- [23] Y. Majdoub, A. Abbou, M. Akherraz, M. El Malah and R. El Akhrif, "Design of an MPPT control under asymmetrical grid faults of DFIG wind turbine," *International Conference on Electrical and Information Technologies (ICEIT)*, 2016, pp. 67-72, doi: 10.1109/EITech.2016.7519563.

- [24] A. Elfadili, F. Giri, H. Ouadi, L. Dugard and A. El Magri, "Induction machine control in presence of magnetic saturation speed regulation with optimized flux reference," *European Control Conference (ECC)*, 2009, pp. 2542-2547, doi: 10.23919/ECC.2009.7074788.
- [25] A. El Fadili *et al.*, "Reference Speed Optimizer Controller for Maximum Power Tracking in Wind Energy Conversion System Involving DFIG," *Renewable Energies, Power Systems & Green Inclusive Economy (REPS-GIE)*, pp. 1-6, 2018, doi: 10.1109/REPSGIE.2018.8488782.
- [26] H. Ouadi, F. Giri, A. Elfadili, Ph. Dorleans, J. F. Massieu, "Induction Machine Control in Presence of Magnetic hysteresis Modelling and Speed reference tracking," *IFAC Proceedings Volumes*, vol. 43, no. 10, pp. 7-12, 2010, doi: 10.3182/20100826-3-TR-4015.00005.

BIOGRAPHIES OF AUTHORS



Youssef Majdoub    received with honors the Ph.D. degree in electrical engineering and advanced controls from Mohammadia School's of Engineers, Rabat, Morocco in 2021. He is currently working as an electrical engineering manager at ONEE-BE (Office National de l'Électricité et de l'Eau Potable-Branche Electricité) in Morocco. He published many papers in international journals and conferences (indexed in SCOPUS). His major areas of interest are: modeling, design and control of the electrical machines, application of power electronics to power systems, and advanced control techniques applied to renewable energy. He can be contacted at email: youssefmajdoub@research.emi.ac.ma.



Ahmed Abbou    received with honors the Ph.D. degree in industrial electronics and electrical machines from Mohammadia School's of Engineers, Rabat, Morocco in 2009. Since 2010, he has been a Professor of Power Electronics and Electric drives at Mohammadia School's of Engineers, Rabat, Morocco. He published more than 170 research papers (indexed in SCOPUS) in international journals, conferences and book chapters on the Electrical machines, Power Electronics and Electrical drives. His current area of interest is related to the innovative control strategies for AC machine, Drives and Renewable Energy. He can be contacted at email: abbou@emi.ac.ma.



Mohamed Akherraz    graduated from the Mohammadia School's of Engineers, Rabat, Morocco in 1980. In 1983 he was granted a Fulbright scholarship to pursue his post-graduate studies. He earned the Ph.D degree in 1987 from UW, Seattle. He joined the EE department of the Mohammadia School's of Engineers, Rabat, Morocco, where he's presently a professor of Power Electronics and Electric drives. He published numerous papers in international journals and conferences. His areas of interests are: Power Electronics, Electric drives, Computer Modeling of Power Electronics circuits, systems and drives. He can be contacted at email: akherraz@emi.ac.ma.